JOINT EUROPEAN TORUS

JET–P(90)20

H.P. Summers, P. Thomas, R. Giannella, M.von Hellermann,
W. Dickson, K. Lawson, W. Mandl, P. Briden and JET Team

Atomic Spectroscopy in Highly Ionised Plasmas

Atomic Spectroscopy in Highly Ionised Plasmas

H.P. Summers, P. Thomas, R. Giannella, M.von Hellermann,
W. Dickson, K. Lawson, W. Mandl, P. Briden and JET Team*

JET-Joint Undertaking, Culham Science Centre, OX14 3DB, Abingdon, UK

** See Appendix 1*

Preprint of Paper to be submitted for publication in
Zeitschrift für Physik

ABSTRACT.

Observations of the JET tokamak are used to illustrate contrasting spectral emission from a range of plasma environments differing in temperature, density, interaction with boundary surfaces, dynamic state and excitation mechanisms. Some spectral features of diagnostic value are identified. Models based on collisional radiative theory are used to investigate these features. The generality of this approach to modelling the radiating properties of atoms in arbitrary dynamic plasmas is indicated.

I. Introduction

The magnetic confinement fusion research machine, JET (Joint European Torus), sustains a plasma composed normally of deuterium, minor impurities such as beryllium, carbon and oxygen and traces of metals such as chromium and nickel at central electron temperatures $\lesssim$12 keV (typically 8 keV) and central electron densities $\lesssim 2\times10^{14}$cm^{-3} (typically 5×10^{13} cm^{-3}). On occasions further gaseous species such as helium are introduced and solid species are (laser) ablated into the plasma. The plasma is optically thin in all impurity radiation. It has strong similarities to astrophysical plasmas such as the solar corona together with some special environments, active control and diagnostic systems which make it a valid and very fruitful source for the study and exploitation of atomic spectroscopy in highly ionised plasmas[1]. This paper rests on a basis of JET spectroscopic observations, however it is believed that the methods used, reliance on and impact on fundamental experimental and theoretical studies of atomic cross-sections etc. are of general relevance.

Figure 1 shows the geometrical layout of JET. The existence of qualitatively distinct radiating zones in the JET plasma arises because of the magnetic field structure and because of the plasma limiting surfaces. Thus, although the bulk plasma, with particle confinement times of order 1 sec radiates in a manner typical of near equilibrium moderate density plasma (albeit at very high temperature), the behaviour of atoms and ions near the edge or in the shadow of limiters is much more dynamic influenced by sources, diffusion and precise plasma positioning. Then again, neutral deuterium heating beams cause profound modification of the radiating behaviour of impurities along or in the locality of the beam lines. Ion cyclotron resonance heating, solid deuterium pellet injection, lower hybrid current drive etc. all alter the radiation emission.

II. Plasma and impurity spectral emission in JET

A VUV survey spectrum is shown in figure 2. It is a radial view across the plasma in the horizontal mid-plane. In this case molybdenum was introduced into a

plasma of central electron temperature ~8 keV by laser ablation. Molybdenum is ionised to approximately the stage Mo^{+40} at this temperature. Lower ionisation stages occur in shells at progressively larger radii from the plasma axis and therefore lower temperature where a balance between ionisation and recombination processes with some influence of diffusion occurs. The deduction of the species concentration from measurement of the line of sight integrated emission in such spectrum lines is the *standard analysis* [2].

Beryllium by contrast is fully ionised throughout virtually the whole plasma. The BeIII emission at 100.26A occurs only at the periphery of the plasma close to the limiting surfaces which are the source of the beryllium. The electron temperature quite close to these surfaces is high compared with the ionisation potential of Be^{+2} and it is probable that Be^{+2} penetrates to such a highly ionising environment before ionisation. Thus the localisation of such an ion is very different resulting from a balance of ionisation and transport processes. The flux of impurities into the plasma and the plasma parameters local to the surfaces which influence impurity release are important matters [3]. Figures 3a and 3b show a high resolution XUV spectrum of BeIII when the plasma was out of and then in contact with the inner wall. Note the singlet series and the intercombination line in figure 3a. The Lyman series of BeIV extends to shorter wavelength, only the first member being present on the spectra. Dynamic state and temperature influence these spectral intensities. Figure 3b introduces a new phenomemon. Disturbance of the series decrement probably indicates the presence of charge transfer reactions from neutral deuterium released from the inner wall by the outward plasma ion flux to it [4].

Visible spectra taken along a horizontal line of sight intersecting and inclined to the neutral heating beam path are shown in figures 4a and 4b. The narrow spectral emission lines in the n = 6-5 principal quantum shell transition of BeIV and in BeII in figure 4b are edge localised emissions similar to those of BeIII in figure 2. The pronounced change in figure 4a in the BeIV lines arises from emission at the beam/viewing line intersection and is driven by charge exchange reactions of Be^{+4} in the core plasma and deuterium in the beams. This is diagnostic of conditions in the plasma centre [5].

Finally figure 5 shows spectra along the same line of sight, but in the wavelength vicinity of D_α at times spanning beam switch on. The charge exchange driven feature at 6561A is similar to that shown in figure 4a above but note the Doppler shifted beam emission split into Stark components by the **vxB** electric field. The principal energy fraction of the beam is at 40 keV/amu, giving electric fields ~100kV/cm. There are also half and third energy components [6]. Excitation of deuterium in the beam is predominantly by plasma ion collisions. The narrow component at 6561A is plasma edge emission in the line of sight. For completeness it should be mentioned that observations of other impurity neutral atom emission, such as BeI and CrI, are also made. Such emission is strongly localised at source surfaces.

The above observations form a connected set linked by atomic reaction processes and by diagnostic usage. Consider firstly the neutral deuterium heating beams. Their penetration into the plasma is a critical parameter. The attenuation is by ionising and charge exchanging collisions with plasma ions (deuterons and impurities) and to a lesser extent by electron collisions. Since it is the simultaneous excitation of the deuterium in the beams which leads to the Stark features, observations such as figure 5 chart the attenuation experimentally. With knowledge of the attenuation, the charge exchange features of figures 5 and 4a allow deduction of absolute radially resolved deuteron and impurity densities. These of course are responsible for the beam attenuation in the first place - a cyclical connection.

The charge exchange features must be separated from superposed cold edge features (figure 4a and 4b). The latter, which are of high principal quantum shell transitions in the visible, are from a complementary cascade path to the resonance lines in the XUV such as shown in figure 3. Excitation of the lower levels of the edge species is principally by electron impact. So the singlet series decrement in figure 3a gives electron temperature. For neutral species, such as Be^0, visible emission is from excited principal quantum shells whose populations are disturbed by further collisions at JET edge densities. So edge electron density is a spectroscopically addressable parameter. The enhancement of the high series members when the plasma is in contact with the inner wall is due to charge transfer from excited states of thermal deuterium near the walls. The excited

deuterium presence is revealed in the Balmer alpha edge emission (figure 5) although the excitation is by electrons rather than ions as was the case for the Stark features. The Stark emission, visible wavelength beam driven charge exchange emission and neutral edge emission are all influenced by higher order collisions with excited states. Such processes also modify the effective attenuation rates for the beams, dielectronic recombination etc. under JET conditions and so ultimately influence ionisation equilibria of impurity ions and the *standard analysis* of eg. Mo^{+30} (figure 2)

III. Interpretative modelling

Formally the line of sight emissivity in the n --> n′ principal quantum shell transition following charge transfer from neutral deuterium in its ground state in the beams to a fully ionised plasma impurity of charge z_0 is

$$I(z,n\text{-->}n') = q_{eff}(z,n\text{-->}n') \int N^{(+z_0)} N_D^{(beam)} dl \qquad (1)$$

where q_{eff} denotes the effective rate coefficient for the particular photon emission and the integral is called the emission measure. z ($=z_0$-1) simply denotes the final charge state. q_{eff} is the derived theoretical quantity which allows the physically useful emission measure to be obtained. That it is not simply the direct charge transfer rate coefficient to the level n times a branching ratio is due to cascade, redistributing secondary collisions etc. It therefore depends on local electron and ion temperature and density as well as beam particle energy. The effective coefficient can appear outside the integral because of the short line-of-sight/beam line intersection. If the attenuated neutral deuterium density at the observed volume is known by calculation or measurement then the emission measure can be resolved to give the impurity density.

Incidentally, the emission measure in equation (1) is almost the same as that involved in formation of the beam Stark emission although in the latter case there is a sum of similar terms for each plasma ion type with appropriate effective

coefficients (driven by ion impact excitation rather than charge exchange) resolved into Stark components (see figure 7).

For emission from a complex (more than one electron) species, X^{+z} (such as Be^{+2}), near the plasma edge, the situation is formally similar to that of equation (1), except that the fundamental driving process is electron impact excitation and the ion species may have significantly populated metastable states, indexed by σ, ($1s^2$ ^1S and $1s2s$ ^3S for Be^{+2}) . Denoting the transition by i--> j for a resolved coupling scheme, then

$$I(z,\sigma,i\text{-->}j) = \int q_{eff}(z,\sigma,i\text{-->}j) N_\sigma^{(+z)} N_e dl \qquad (2)$$

with a different differential emission measure $N_\sigma^{(+z)} N_e dl$ where $N_\sigma^{(+z)}$ denotes the density of ions in the metastable state σ. The view of metastable populations as quasi-independent is somewhat different from the usual astrophysical approach in which an ionisation balance assumption is made and then $N_\sigma^{(+z)} / N_{tot}$ incorporated with q_{eff} giving a '$g(T_e)$' function [8]. The present is the more general case and is certainly appropriate at the periphery of JET where collisional mixing timescales for ground and metastable populations are comparable with diffusion and dynamical timescales. This is illustrated in figure 8. The JET data (see figure 3a) matches the transient case.

For inflowing atoms or ions from localised surfaces ionising fully near the surface without dispersion , the flux can be related to the emission along a line of sight orthogonal to the surface from any one of its ionisation stages as

$$\Gamma = \Sigma_\sigma \Gamma(z,\sigma) = \Sigma_\sigma E(z,\sigma,i\text{-->}j)\, I(z,\sigma,i\text{-->}j) \qquad (3)$$

where $\Gamma(z,\sigma)$ is the partial flux in metastable state σ of the impurity ion of charge state z. E is the number of ionisations per photon or the reciprocal of the *photon efficiency* and is the relevant derived theoretical quantity needed for interpretation. An observed spectral intensity is associated with each metastable. In general the photon efficiency also depends on density as well as temperature particularly for species in neutral or near neutral stages of ionisation.

IV. The unified picture

The effective coefficients used in the above studies were obtained by collisional radiative population calculations[9]. In these it was necessary to compute both large sets of principal quantum shell ('bundle-n') [10] populations and large sets of ('resolved') low level populations of ions - the latter with precision. In some cases, high level bundle-n calculations were coupled to low level resolved calculations. Complex ions had to be addressed and metastable states distinquished.

The theoretical picture can be completed by considering ionisation and recombination. Then the evolution of ionisation stage populations into each other can be modelled. It is at this point that usages for general plasma simulations and detailed interpretative spectroscopy tend to be most discordant. Properly, each stage must be represented by its ground and metastable populations and the effective ('generalised collisional dielectronic') coefficients established between them, namely $\alpha_{cd}(z+1,\rho';z,\rho)$, $S_{cd}(z,\rho;z+1,\rho')$ and the cross-coupling coefficients $q_{cd}(z,\rho;z,\sigma)$. They depend on density as well as temperature. It was these coefficients which were used for figure 8. Supplemented with power loss coefficients they provide the effective atomic source terms for arbitrary finite density dynamic plasma theoretical simulations matching spectroscopy[11].

On a theoretical note, the detailed effective emission coefficients and the generalised collisional dielectronic coefficients can be computed simultaneously. The procedures upon which this work draws organise recombining ion metastable (parent) and recombined ion spin system resolved bundle-n calculations to provide projection matrices which are expanded over resolved low level manifolds and combined with high quality low level rates from assessed atomic data bases. Subsequent matrix manipulations yield all relevant quantities.

V. Conclusion

In this paper spectrocopic observation and detailed interpretative atomic modelling have been closely linked. It has served to clarify a framework and quality of derived atomic data structures appropriate both for diagnostic spectroscopy and general plasma simulation. The starting point is however electron/atom, atom/ion and atom/atom collision data of good reliability. This paper can be seen as one view of how to make best use of spectroscopic observations and fundamental data in a fusion plasma context.

References

1. JET Progress Report, EUR 12808 EN, EUR-JET-PR7 (1989)
2. Behringer K., Engelhardt W.W., Horton L. et al.: Proc XIII Symposium on Physics of Ionised Gases, Yugoslavia (1986)
3. Behringer K.H., Summers H.P., Denne B., Forrest M. & Stamp M.F.: Plasma Phys. & Contr. Fusion **31**, 2059 (1989)
4. Mattioli M., Peacock N.J., Summers H.P., Denne B. & Hawkes N.C.: Phys. Rev. **A40**, 3886 (1989)
5. Boileau A., von Hellermann M., Horton L.D. & Summers H.P.: Plasma Phys & Contr. Fusion **31**, 779 (1989)
6. Boileau A., von Hellermann M., Mandl W., Summers H.P., Weisen H. & Zinoviev A.: J Phys B **22**, 1145 (1989)
7. Summers H.P., Behringer K.H. & Wood L.: Physica Scripta **35**, 303 (1987)
8. Lang J., McWhirter R.W.P. & Mason H.: Solar Physics - in press (1990)
9. Bates D.R., Kingston A.E. & McWhirter R.W.P.: Proc. Roy. Soc. **A276**,297 (1962)
10. Burgess A. & Summers H.P.: Mon. Not. R. Astr. Soc. **226**,257 (1987)
11. Summers H.P. & Hooper M.B.: Plasma Physics **25**,1311 (1983)

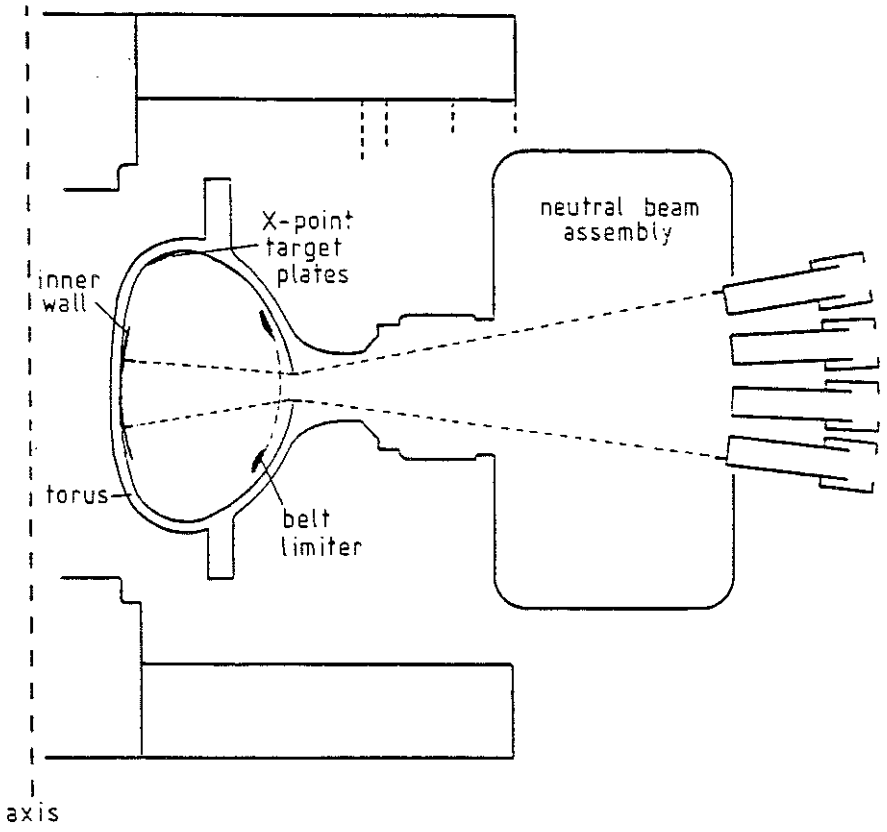

Fig. 1. A vertical section of JET. Note the graphite tile protected inner wall, beryllium belt limiters and the neutral beam injector (NBI) assembly.

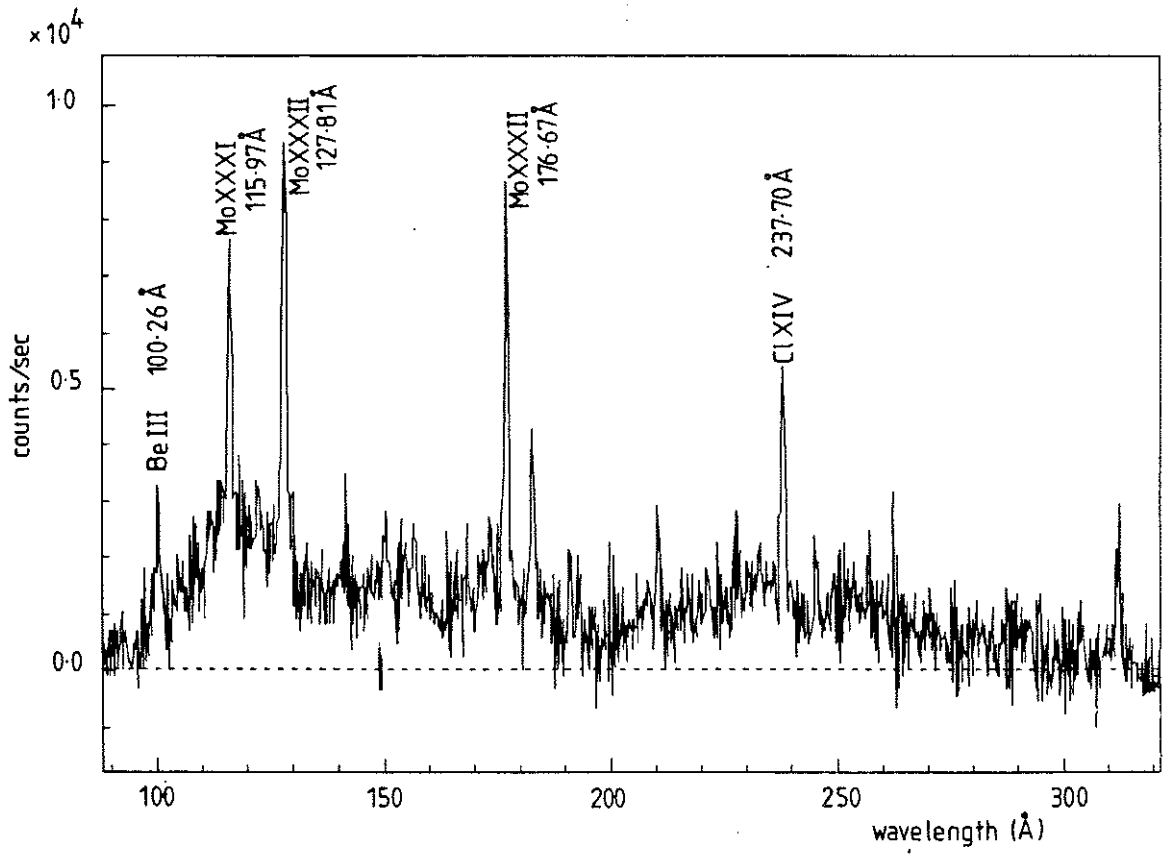

Fig. 2. Survey spectrum in the VUV spectral region.

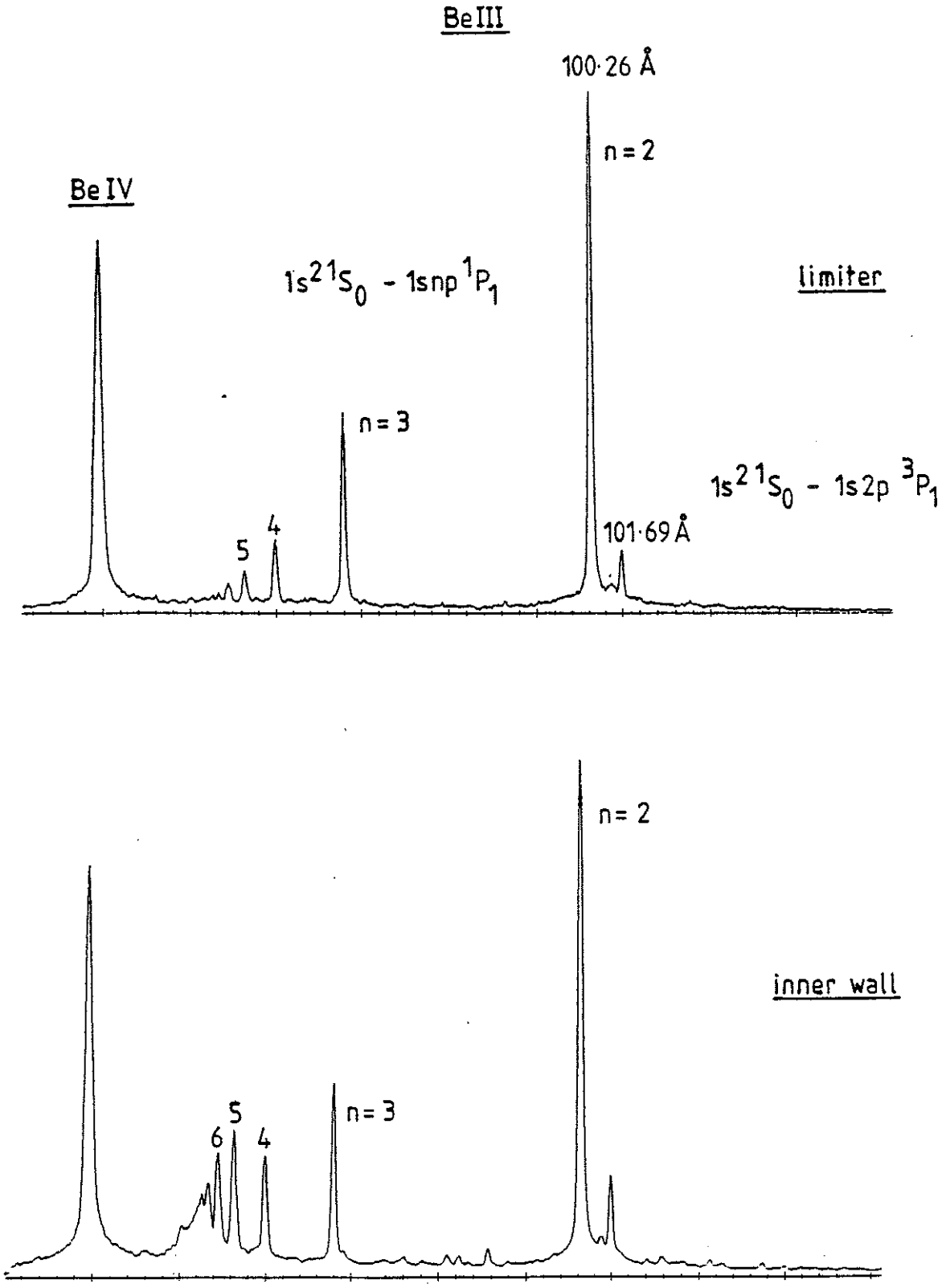

Fig. 3. XUV spectrum along a line of sight directed at the inner wall: (a) Plasma in contact with the outer belt limiters.(b) Plasma in contact with the inner wall.

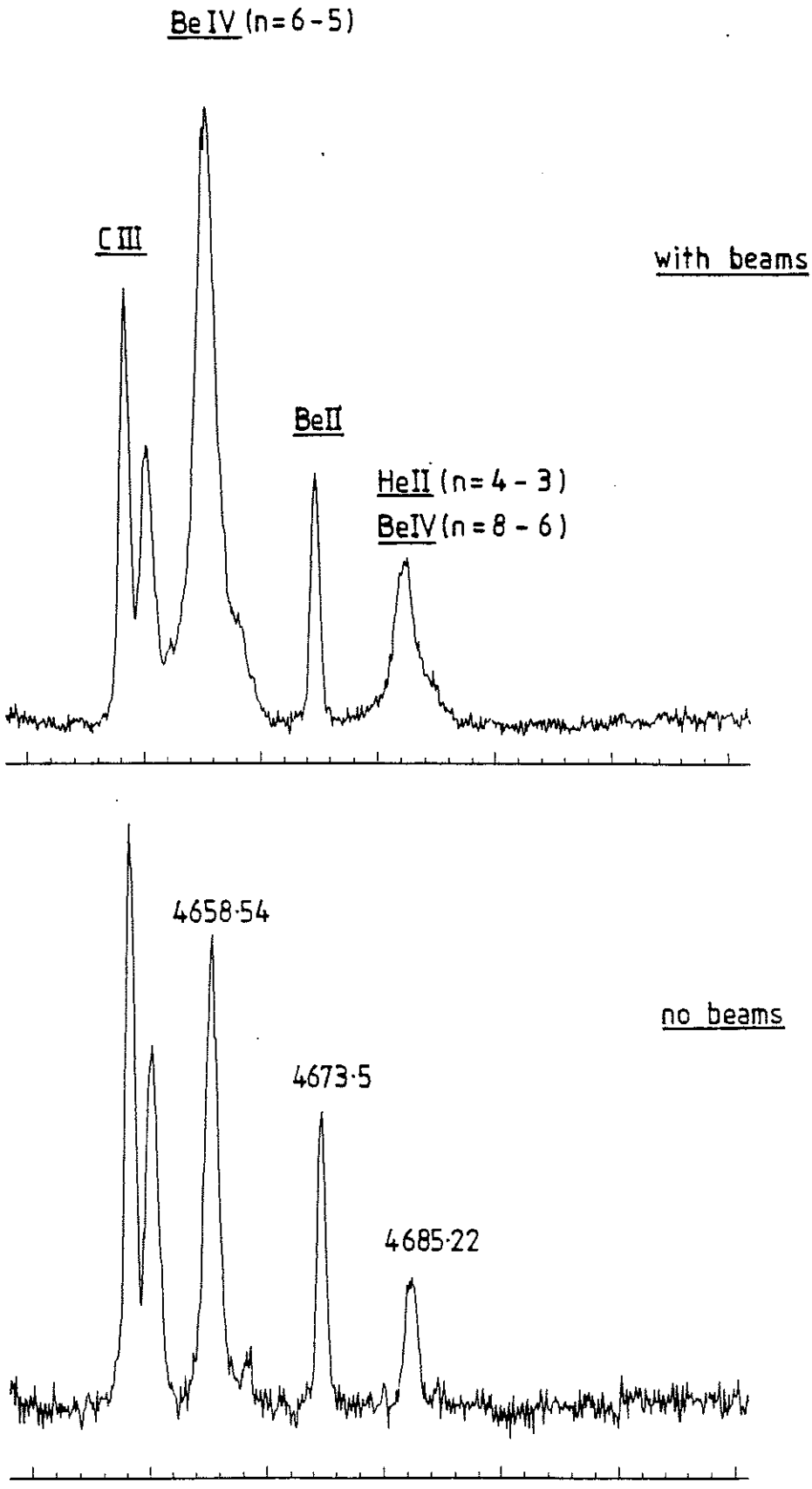

Fig. 4. Visible spectrum along a line of sight intersecting the neutral deuterium beams: (a) Beams active, (b) Beams inactive.

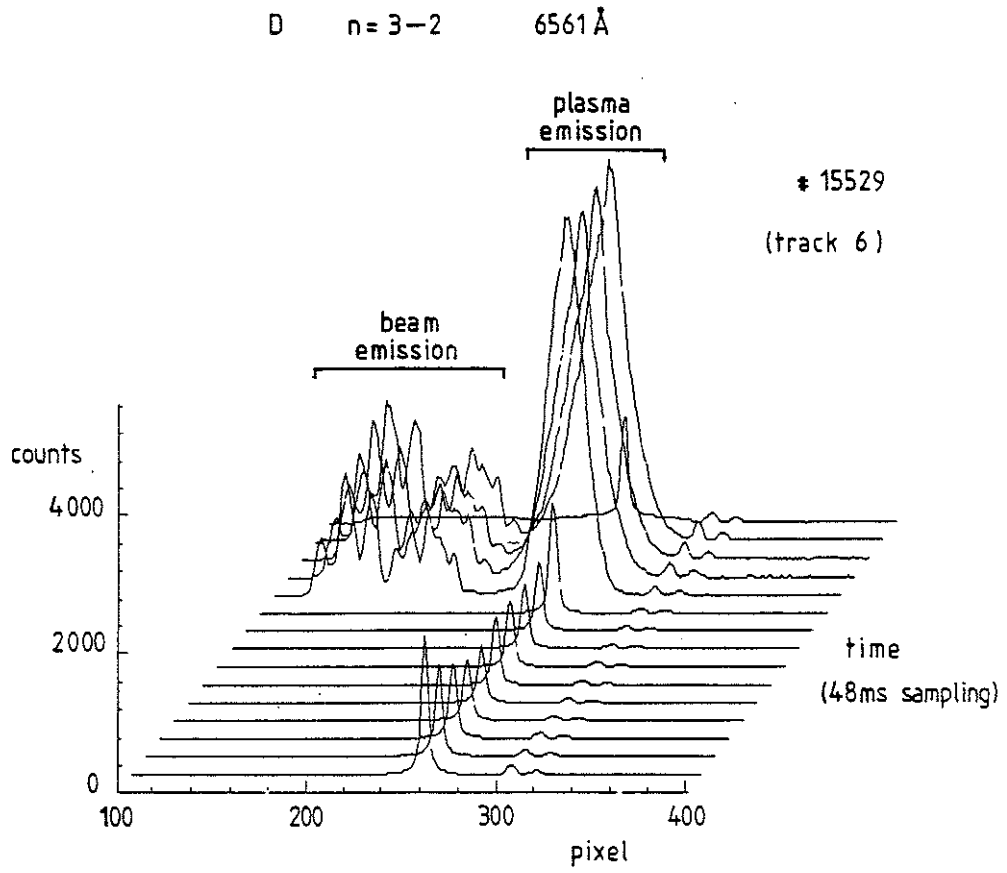

Fig. 5. Visible spectrum along a line of sight intersecting the neutral deuterium beams

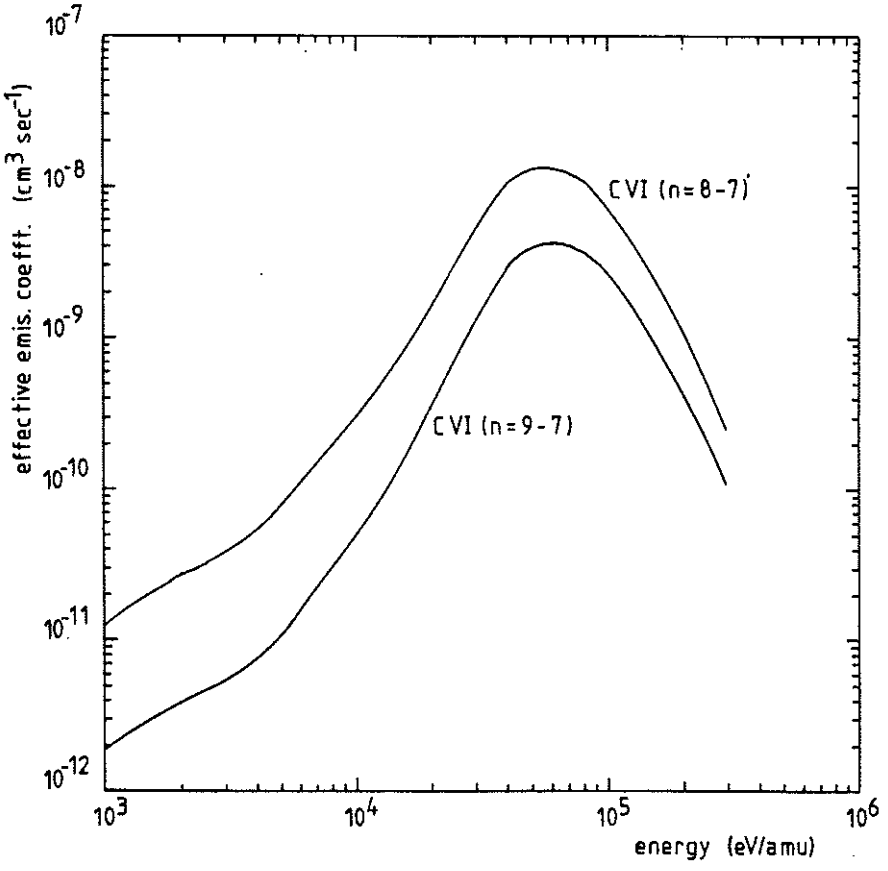

Fig. 6. Charge exchange effective emission coefficients for CVI(n=8-7) & CVI(n=9-7) at $T_i = 5000$eV, $N_i = 2.0 \times 10^{13}$ cm^{-3}, $Z_{eff} = 2$.

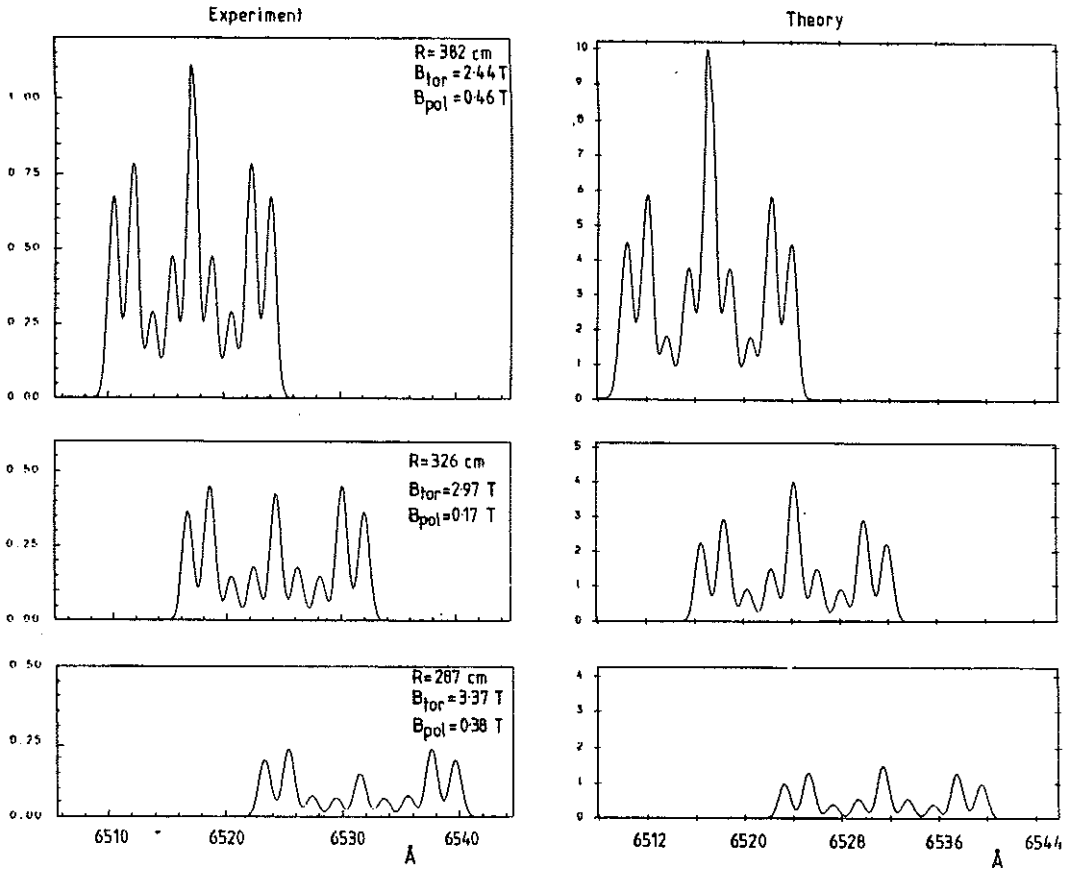

Fig. 7. Comparison of the measured primary energy Stark features, isolated by multiple Gaussian fiiting procedures with the modelled features normalised to each other at r/a = 0.7, where a is the horizontal semi-major axis.

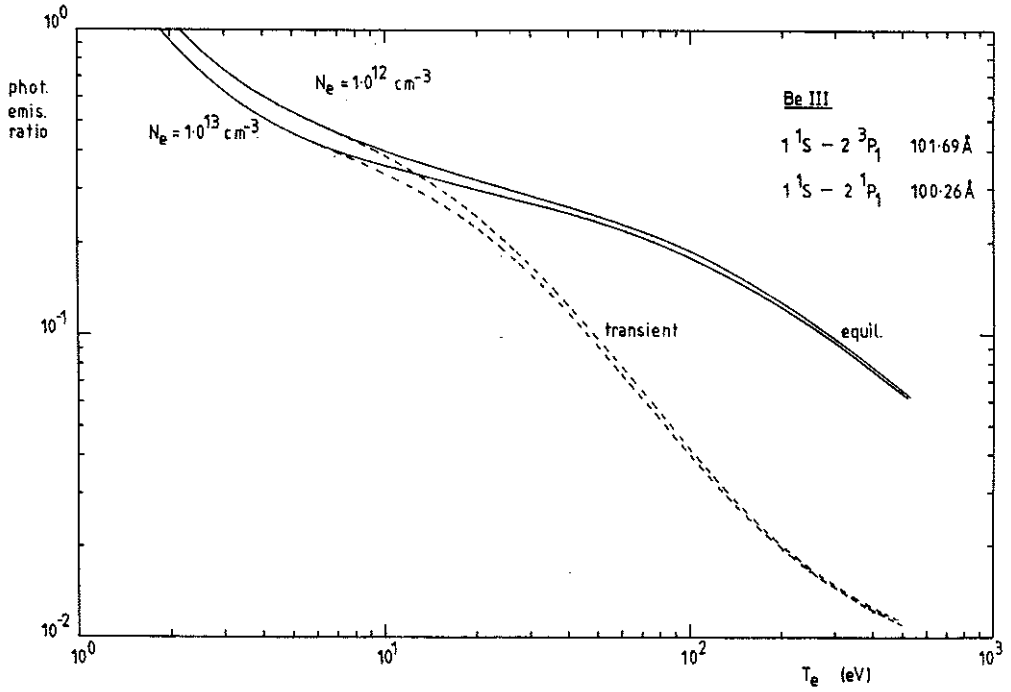

Fig. 8. Emissivity ratio for BeIII ($1s^2\,{}^1S$ - $1s2p\,{}^1P$) and BeIII ($1s^2\,{}^1S$ - $1s2p\,{}^3P$). The transient case assumes evolution from Be^{+1} to Be^{+4} in a plasma of specified temperature and the time integrated emissivity ratio is given.

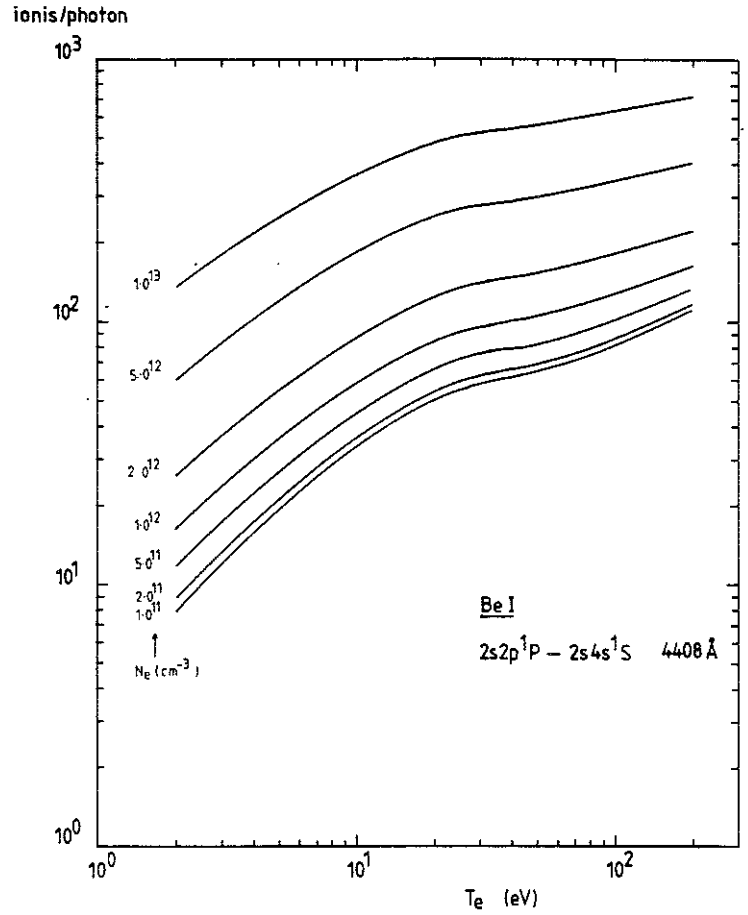

Fig. 9. Ionisations per photon for BeI 4408A. corresponding to the transition 2s4s ^{1}S - 2s2p ^{1}P.

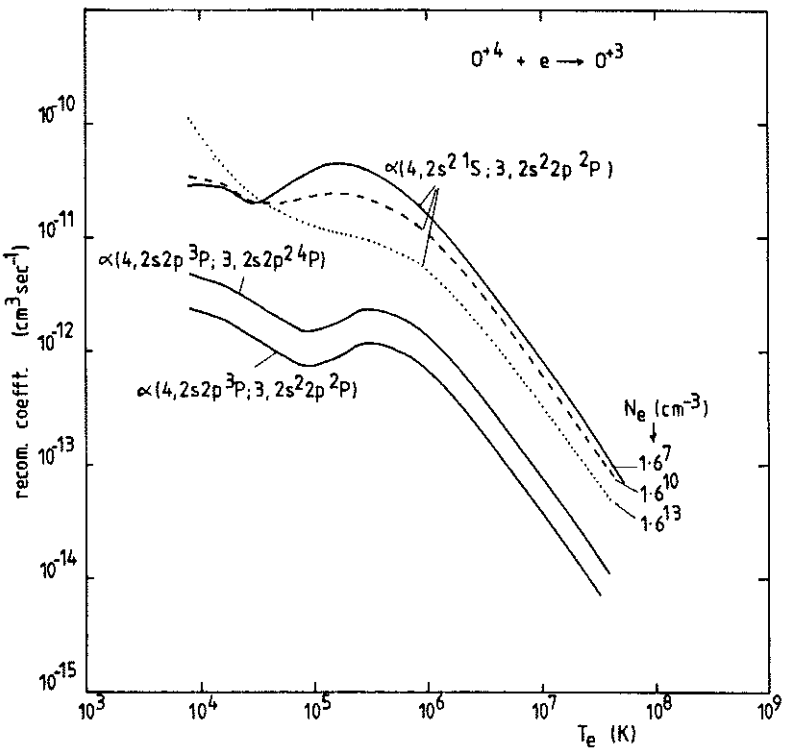

Fig. 10. Generalised collisional-dielectronic recombination coefficients for O^{+4} + e ---> O^{+3}

APPENDIX 1.

THE JET TEAM

JET Joint Undertaking, Abingdon, Oxon, OX14 3EA, U.K.

J.M.Adams[1], F.Alladio[4], H.Altmann, R.J.Anderson, G.Appruzzese, W.Bailey, B.Balet, D.V.Bartlett, L.R.Baylor[24], K.Behringer, A.C.Bell, P.Bertoldi, E.Bertolini, V.Bhatnagar, R.J.Bickerton, A.Boileau[3], T.Bonicelli, S.J.Booth, G.Bosia, M.Botman, D.Boyd[31], H.Brelen, H.Brinkschulte, M.Brusati, T.Budd, M.Bures, T.Businaro[4], H.Buttgereit, D.Cacaut, C.Caldwell-Nichols, D.J.Campbell, P.Card, J.Carwardine, G.Celentano, P.Chabert[27], C.D.Challis, A.Cheetham, J.Christiansen, C.Christodoulopoulos, P.Chuilon, R.Claesen, S.Clement[30], J.P.Coad, P.Colestock[6], S.Conroy[13], M.Cooke, S.Cooper, J.G.Cordey, W.Core, S.Corti, A.E.Costley, G.Cottrell, M.Cox[7], P.Cripwell[13], F.Crisanti[4], D.Cross, H.de Blank[16], J.de Haas[16], L.de Kock, E.Deksnis, G.B.Denne, G.Deschamps, G.Devillars, K.J.Dietz, J.Dobbing, S.E.Dorling, P.G.Doyle, D.F.Düchs, H.Duquenoy, A.Edwards, J.Ehrenberg[14], T.Elevant[12], W.Engelhardt, S.K.Erents[7], L.G.Eriksonn[5], M.Evrard[2], H.Falter, D.Flory, M.Forrest[7], C.Froger, K.Fullard, M.Gadeberg[11], A.Galetsas, R.Galvao[8], A.Gibson, R.D.Gill, A.Gondhalekar, C.Gordon, G.Gorini, C.Gormezano, N.A.Gottardi, C.Gowers, B.J.Green, F.S.Griph, M.Gryzinski[26], R.Haange, G.Hammett[6], W.Han[9], C.J.Hancock, P.J.Harbour, N.C.Hawkes[7], P.Haynes[7], T.Hellsten, J.L.Hemmerich, R.Hemsworth, R.F.Herzog, K.Hirsch[14], J.Hoekzema, W.A.Houlberg[24], J.How, M.Huart, A.Hubbard, T.P.Hughes[32], M.Hugon, M.Huguet, J.Jacquinot, O.N.Jarvis, T.C.Jernigan[24], E.Joffrin, E.M.Jones, L.P.D.F.Jones, T.T.C.Jones, J.Källne, A.Kaye, B.E.Keen, M.Keilhacker, G.J.Kelly, A.Khare[15], S.Knowlton, A.Konstantellos, M.Kovanen[21], P.Kupschus, P.Lallia, J.R.Last, L.Lauro-Taroni, M.Laux[33], K.Lawson[7], E.Lazzaro, M.Lennholm, X.Litaudon, P.Lomas, M.Lorentz-Gottardi[2], C.Lowry, G.Magyar, D.Maisonnier, M.Malacarne, V.Marchese, P.Massmann, L.McCarthy[28], G.McCracken[7], P.Mendonca, P.Meriguet, P.Micozzi[4], S.F.Mills, P.Millward, S.L.Milora[24], A.Moissonnier, P.L.Mondino, D.Moreau[17], P.Morgan, H.Morsi[14], G.Murphy, M.F.Nave, M.Newman, L.Nickesson, P.Nielsen, P.Noll, W.Obert, D.O'Brien, J.O'Rourke, M.G.Pacco-Düchs, M.Pain, S.Papastergiou, D.Pasini[20], M.Paume[27], N.Peacock[7], D.Pearson[13], F.Pegoraro, M.Pick, S.Pitcher[7], J.Plancoulaine, J-P.Poffé, F.Porcelli, R.Prentice, T.Raimondi, J.Ramette[17], J.M.Rax[27], C.Raymond, P-H.Rebut, J.Removille, F.Rimini, D.Robinson[7], A.Rolfe, R.T.Ross, L.Rossi, G.Rupprecht[14], R.Rushton, P.Rutter, H.C.Sack, G.Sadler, N.Salmon[13], H.Salzmann[14], A.Santagiustina, D.Schissel[25], P.H.Schild, M.Schmid, G.Schmidt[6], R.L.Shaw, A.Sibley, R.Simonini, J.Sips[16], P.Smeulders, J.Snipes, S.Sommers, L.Sonnerup, K.Sonnenberg, M.Stamp, P.Stangeby[19], D.Start, C.A.Steed, D.Stork, P.E.Stott, T.E.Stringer, D.Stubberfield, T.Sugie[18], D.Summers, H.Summers[20], J.Taboda-Duarte[22], J.Tagle[30], H.Tamnen, A.Tanga, A.Taroni, C.Tebaldi[23], A.Tesini, P.R.Thomas, E.Thompson, K.Thomsen[11], P.Trevalion, M.Tschudin, B.Tubbing, K.Uchino[29], E.Usselmann, H.van der Beken, M.von Hellermann, T.Wade, C.Walker, B.A.Wallander, M.Walravens, K.Walter, D.Ward, M.L.Watkins, J.Wesson, D.H.Wheeler, J.Wilks, U.Willen[12], D.Wilson, T.Winkel, C.Woodward, M.Wykes, I.D.Young, L.Zannelli, M.Zarnstorff[6], D.Zasche[14], J.W.Zwart.

PERMANENT ADDRESS

1. UKAEA, Harwell, Oxon. UK.
2. EUR-EB Association, LPP-ERM/KMS, B-1040 Brussels, Belgium.
3. Institute National des Récherches Scientifique, Quebec, Canada.
4. ENEA-CENTRO Di Frascati, I-00044 Frascati, Roma, Italy.
5. Chalmers University of Technology, Göteborg, Sweden.
6. Princeton Plasma Physics Laboratory, New Jersey, USA.
7. UKAEA Culham Laboratory, Abingdon, Oxon. UK.
8. Plasma Physics Laboratory, Space Research Institute, Sao José dos Campos, Brazil.
9. Institute of Mathematics, University of Oxford, UK.
10. CRPP/EPFL, 21 Avenue des Bains, CH-1007 Lausanne, Switzerland.
11. Risø National Laboratory, DK-4000 Roskilde, Denmark.
12. Swedish Energy Research Commission, S-10072 Stockholm, Sweden.
13. Imperial College of Science and Technology, University of London, UK.
14. Max Planck Institut für Plasmaphysik, D-8046 Garching bei München, FRG.
15. Institute for Plasma Research, Gandhinagar Bhat Gujat, India.
16. FOM Instituut voor Plasmafysica, 3430 Be Nieuwegein, The Netherlands.
17. Commissiariat à L'Energie Atomique, F-92260 Fontenay-aux-Roses, France.
18. JAERI, Tokai Research Establishment, Tokai-Mura, Naka-Gun, Japan.
19. Institute for Aerospace Studies, University of Toronto, Downsview, Ontario, Canada.
20. University of Strathclyde, Glasgow, G4 ONG, U.K.
21. Nuclear Engineering Laboratory, Lapeenranta University, Finland.
22. JNICT, Lisboa, Portugal.
23. Department of Mathematics, Univeristy of Bologna, Italy.
24. Oak Ridge National Laboratory, Oak Ridge, Tenn., USA.
25. G.A. Technologies, San Diego, California, USA.
26. Institute for Nuclear Studies, Swierk, Poland.
27. Commissiariat à l'Energie Atomique, Cadarache, France.
28. School of Physical Sciences, Flinders University of South Australia, South Australia SO42.
29. Kyushi University, Kasagu Fukuoka, Japan.
30. Centro de Investigaciones Energeticas Medioambientales y Techalogicas, Spain.
31. University of Maryland, College Park, Maryland, USA.
32. University of Essex, Colchester, UK.
33. Akademie de Wissenschaften, Berlin, DDR.

CR 88.49.1A